PNAS RESEARCH ARTICLE | APPLIED PHYSICAL SCIENCES OPEN ACCESS

Optimal disk packing of chloroplasts in plant cells

Nico Schramma[a], Eric R. Weeks[b], and Maziyar Jalaal[a,1]

Edited by Salvatore Torquato, Princeton University Department of Chemistry, Princeton, NJ; received May 9, 2025; accepted September 18, 2025 by Editorial Board Member Daan Frenkel

Photosynthesis is essential for ecosystem survival, but while plants require light, excessive exposure can damage cells. Chloroplasts, photosynthetic organelles, respond via self-organized motion within cells to optimize light absorption. These disk-shaped organelles must balance two competing needs: dense packing to enhance absorption under dim light and rapid spatial rearrangement to avoid damage from excess light. Using microscopy, we show that plant cell shape and chloroplast size achieve both goals: dense monolayer packing for optimal absorption in low light and sidewall packing for light avoidance. We present a theoretical model using random close packing simulations of polydispersed hard disks in rectangular boxes and find optimal cell shapes that match plant cell measurements. Our findings highlight how particle packing principles under confinement enable light adaptation in plants, offering insights into organelle organization under confinement, a physical challenge relevant across biological systems.

packing | chloroplast photoadaptation | plant physics | jamming | cell structure

Significance

Plant cells face a trade-off between capturing enough light for photosynthesis and avoiding damage from too much sunlight. Their adaptation mechanism includes active rearrangements of disk-shaped chloroplasts, spreading them out under dim light to maximize absorption, then stacking them along the cells' side walls under intense light to reduce photodamage. But how is such intracellular reorganization facilitated? In the aquatic plant *Elodea densa*, we find that the shape and size of leaf-cells are optimized so that chloroplasts pack optimally in a single layer, yet can still dynamically relocate to the walls when needed. By combining live-cell imaging with computer simulations of disks confined in a box, we show that this dynamic behavior rests on fundamental principles of disk-packing physics.

Photosynthesis is a fundamental process necessary for most life on Earth. However, fluctuations in light impose significant stress on plants, necessitating permanent dynamic adaptation. In addition to exhibiting macroscopic movements, such as phototropism, heliotropism, and shade avoidance (1–4), photosynthetic organisms are also capable of changing their intracellular structure (5), for example, by moving chloroplasts in response to light (6–10). In plants, disk-shaped chloroplasts, responsible for photosynthesis, can move toward or away from light by actively assembling networks of short actin filaments around them (8, 11–15), allowing them to collectively rearrange the intracellular structure to tune the optical properties of plant cells (7, 16, 17). Dim light eventually leads to an accumulation of chloroplasts in a layer to maximize the absorption of light (18), while in strong light, chloroplasts move toward the sidewalls to increase leaf transmittance and avoid photodamage, such as increased production of reactive oxygen species (6, 19–23). Although the molecular driving mechanisms of these movements are well studied, the collective aspects of the large-scale rearrangement motion of chloroplasts in plant cells remain enigmatic.

How do cell shape and size impact the ability of the relatively large number ($N \approx 50$ to 120) of chloroplasts to collectively rearrange the intracellular structure to achieve various packing configurations for light adaptation? Waterplants such as *Elodea densa*, the subject of this study, provide an optimal system for microscopically studying chloroplast motion due to their simple two-cell-layered leaf structure. In a previous study, we identified a glass-like state under dim light conditions, where chloroplasts in a dense two-dimensional configuration (packing fraction $\phi \approx 70$ to 74%) are caged and unable to move freely, exhibiting dynamics similar to those in glassy systems (9). These mechanical characteristics stem from the high two-dimensional density of chloroplasts, which are bound to mostly move on the inner walls of the cells, as their movement relies on the anchorage to the plasma membrane (8, 24), which can be alleviated via blue light in water plants (25–28). Upon strong light stimulation, the organelles become highly active and quickly transition within tens of minutes out of this two-dimensional glassy regime into a three-dimensional collective swirling motion of aggregates. These aggregates eventually spread on the side walls, enabling light avoidance (Movie S1).

While the dynamic phases themselves pose intriguing questions about photoactivated phase transitions in a biological active matter system under confinement, several questions remain open regarding the underlying geometric aspects of chloroplast packing within cell confinement. In fact, the dynamic adaptation response is infeasible if chloroplast number or size is altered. Normally, chloroplasts reach 2D packing densities of $\phi \approx 54\%$ in spinach, 63% in beetroot (29), 69% in wheat (30) and around 80% in *Arabidopsis* (31), with their number correlating to the area of their cells (29, 30) and chloroplast size (32).

It was found that a few enlarged chloroplasts cannot rearrange within the cell to reduce photodamage efficiently (33, 34), while a large population of smaller chloroplasts

Author affiliations: [a]Van der Waals-Zeeman Institute, Institute of Physics, University of Amsterdam, Amsterdam 1098XH, The Netherlands; and [b]Department of Physics, Emory University, Atlanta, GA 30322

Author contributions: N.S. and M.J. designed research; N.S. and E.R.W. performed research; N.S. contributed new reagents/analytic tools; N.S. and E.R.W. analyzed data; E.R.W. performed simulations; and N.S. and M.J. wrote the paper.

The authors declare no competing interest.

This article is a PNAS Direct Submission. S.T. is a guest editor invited by the Editorial Board.

[1]To whom correspondence may be addressed. Email: m.jalaal@uva.nl.

This article contains supporting information online at https://www.pnas.org/lookup/suppl/doi:10.1073/pnas.2511696122/-/DCSupplemental.

Published October 22, 2025.

performs better (35–38). These studies suggest that chloroplast size might be optimal for photosynthesis (39) and is crucial to be well controlled. Importantly, not only chloroplast number and size but also the cell shape have an impact on this adaptation response; for example, in lobed cells of *Magnolia* or *Zamia* leaves, chloroplasts cannot rearrange efficiently (7). These findings lead to the hypothesis that alterations to cell size and shape play a significant role in controlling the photoprotection efficiency.

Here, we study the interplay between cell geometry and chloroplast size to determine balanced packing to achieve optimal light harvest and photoavoidance motion in the cuboid cells of the waterplant *E. densa*. To accomplish this, we model chloroplast packing structures as a disk packing problem of two-dimensional polydisperse disks in rectangular confinement. The optimal packing of n-dimensional spheres ($n \geq 2$) is a century-old problem with wide-ranging applications in condensed matter systems (40–42), optimization (43), and signal transduction (44, 45). The complexity of this seemingly simple problem is evident in the case of monodisperse spheres in three-dimensional free space. The optimal packing was conjectured to be a face-centered cubic structure by Johannes Kepler in 1611 (46) [but studied centuries earlier in a Sanskrit work "ĀryabhatĪya of Āryabhata" from 499 CE (47)] and was ultimately proven almost 400 y later by Thomas Hales in 1998 (40, 48). Notably, packing (or tiling) constituents in living materials, similar to many classical condensed matter systems, feature additional complexities. First, in most cases, the packing is disordered, lacking a clear crystalline structure or consisting of building blocks with more complex shapes (49–55).

In the presence of noise and size-polydispersity, maximally dense packings can be determined algorithmically. However, the random close packing density ϕ_{rcp} is not well-defined and depends not only on particle shape (56, 57) and size distribution (58–60) but also on the choice of the algorithm used (61–63). Second, biological systems are often highly geometrically confined. Such a constraint strongly affects packing (64–66) and transport (67) and may induce phase transitions by lowering their critical density (68–74).

By studying chloroplast configurations through the classical perspective of a packing problem, we aim to uncover critical dependencies between chloroplast size and cell shape. To achieve this, this work is divided into three parts: First, we quantify and describe the structure of cells in our model system. Next, we introduce the disk packing simulation based on experimental parameters. Finally, we construct two arguments for maximal packing in the cells' center and the side walls, which, when combined, define a clear optimal shape.

Disk-Shaped Chloroplasts Are Confined in Elongated Rectangular Cells

We study the cell shape and structure of the water plant *E. densa*, commonly referred to as "waterpest," using bright-field and confocal fluorescence microscopy. This monocot plant has a simple structure characterized by fourfold symmetric leaf arrangements on a single stalk (Fig. 1*A*). The leaves have two layers: an adaxial (*Upper*) layer with larger cells and an abaxial

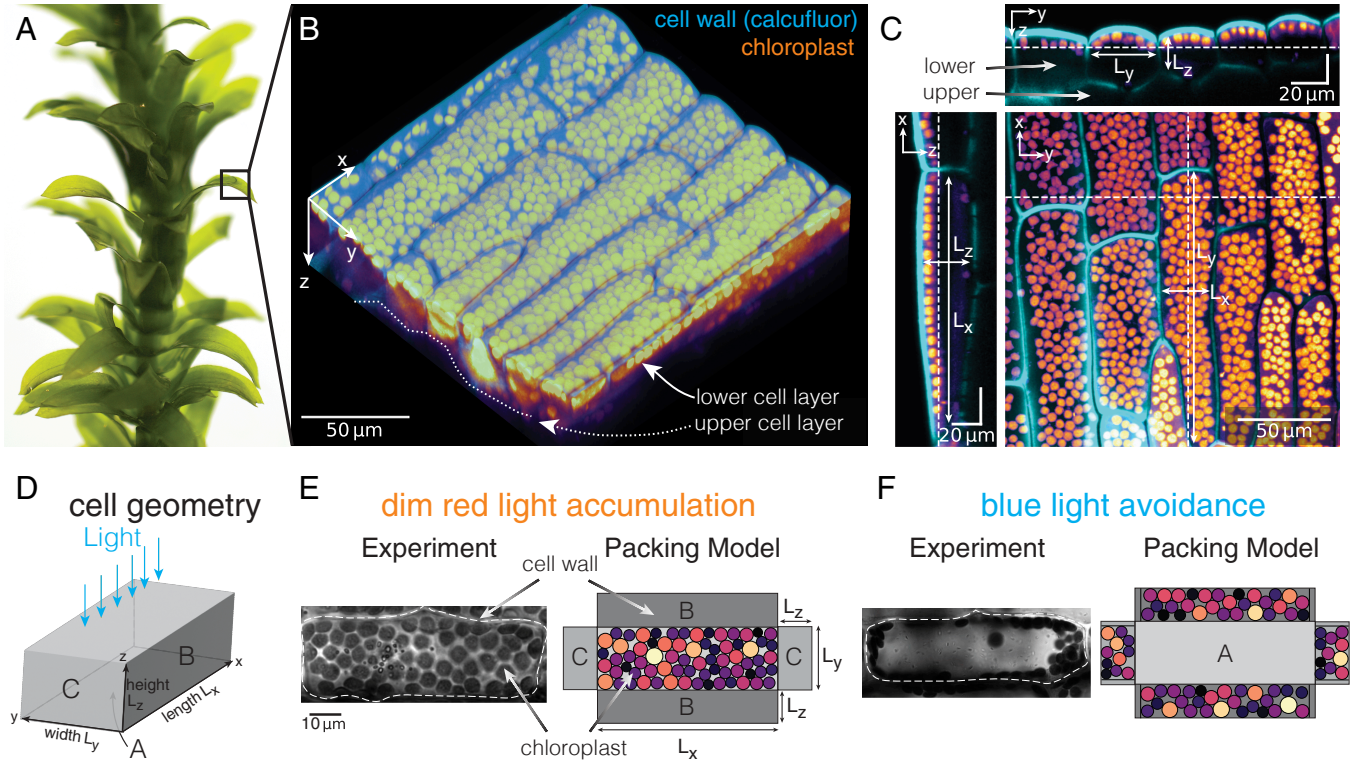

Fig. 1. Overview of experiment and packing model. (*A*) The aquatic plant *Elodea densa*. (*B*) A 3D confocal image of the cell walls shows a bilayered leaf structure. We focus on the abaxial (*Lower*) cell layer, depicted on *Top*. Cyan channel: cell wall. Disk-like green structures: chloroplasts. Dotted line: guide to the eye to distinguish abaxial (*Lower*) from adaxial (*Upper*) cell layer. (*C*) Orthogonal view of cell walls (cyan) and chloroplasts (orange) along dotted white lines, respectively. Walls represent box-like structures with definitions of the box length L_x, width L_y, and height L_z of the *Lower* cell layer. (*D*) Schematic of the box geometry and experiment. Light enters from the *Top*. *Bottom* wall A and sidewalls B and C are shown. (*E*) Cells under weak red light: Chloroplasts are packed with a high density on the *Bottom* wall. The packing model (*Right*) shows a schematic of the opened box with chloroplasts packed solely in the A-plane. (*F*) Cells under strong blue light: Chloroplasts spread on the side walls B and C. In the model, the chloroplasts are packed on B and C planes. A brighter color corresponds to larger chloroplasts.

(*Lower*) layer with cells approximately half the size (Fig. 1 *B* and *C* and *SI Appendix*, Fig. S1) (75, 76) [similar to the related plant *Elodea canadensis* (77)]. We observe that upon strong light stimulation, the disk-shaped chloroplasts in the *Bottom* of the cell move toward the side walls after creating a motile aggregate (Fig. 1 *D–F* and *SI Appendix*, Fig. S2 and Movie S1).

To quantify the cell shapes and chloroplast sizes, we perform bright-field imaging and chlorophyll autofluorescence microscopy (*Materials and Methods*, *SI Appendix*, Fig. S3). We analyze 262 cuboid-shaped cells and $n = 4{,}451$ disk-shaped chloroplasts (in 59 cells), with an approximately Gaussian-distributed disk-radius $r = 2.12 \pm 0.29\,\mu\text{m}$ (mean ± SD) and polydispersity $\delta = \langle r\rangle/\sigma_r = 13.6\,\%$ and with an aspect ratio close to 1 (Fig. 2*A*).

We find scaling between cell area $\mathcal{A}$ and chloroplast number N (Fig. 2*B*), consistent with previous observations in other plants (29, 30, 32, 39). As chloroplasts in dim light mostly pack in a single layer, the upper limit of this scaling is expected to result from random close packing in two-dimensional free space with a packing density ϕ_{rcp} (dotted line in Fig. 2*B*). However, the chloroplast number lies well below this line, which likely results from the dependency of random close packing on the confinement (64). Furthermore, we find that cells have various lengths $L_x = 50$ to $125\,\mu\text{m}$ while their width remains largely constant $L_y = 22.2 \pm 2.95\,\mu\text{m}$ (Fig. 2*C*).

To provide a physical intuition about the cell confinement, we rescale all dimensions by the average chloroplast diameter $2\langle r\rangle$. This renders all length scales in terms of the average number of chloroplasts that fit within a given space and suggests that only 4 to 7 chloroplasts fit within the width of the cells, while the cell length varies between approximately 10 to 30 chloroplasts. To measure the height of the cuboid cells, we stain the cell walls with calcofluor and perform confocal microscopy to generate three-dimensional volumetric images of the plant cells (*Materials and Methods*). We find that the cells have an average height $L_z/2\langle r\rangle \approx 2.34 \pm 1$ ($n = 86$) measured within one average chloroplast diameter from the boundary (compare Fig. 1*C* and *SI Appendix*, Fig. S2 *C* and *D*). Notably, sometimes the lower cell walls align with the upper cells, creating trapezoidal shapes in which one cell wall is much higher than the other. Taken together, this shows that chloroplasts are highly confined in two directions and have greater freedom to arrange along the long side of the cell. With these insights about chloroplast size and the respective confinement, we ask whether these sizes are optimally related to achieving both objectives: optimal light capture and optimal chloroplast avoidance. To address this, we will present a theoretical argument in the next section.

2D Chloroplast Packing in Confinement

It has been observed that chloroplasts move toward the bottom wall under dim light and toward the sidewalls under strong light (8, 26, 35, 78) (Fig. 1 *E* and *F*), with each configuration—chloroplasts in a single bottom layer or at the sidewalls—serving distinct purposes for light adaptation. The first is associated with the optimal light uptake under dim conditions (18), while the latter is a light-avoidance response that optimizes the intracellular structure for enhanced light transmission and thus reduced photodamage (6, 7, 17). Notably, a large volume of the cell is occupied by the central vacuole, allowing chloroplasts to only move in two dimensions.

To outline the interplay of chloroplast number, size, and cell geometry, let us consider a cuboid cell (container) shaped to allocate many disk-shaped chloroplasts in the *Bottom* layer (Fig. 1 *D–F*). If the side walls are not large enough to accommodate all chloroplasts during strong light avoidance, excessive light exposure may harm the chloroplasts (20, 21). This happens if the cuboid has a square-shaped top and bottom face and is rather flat. On the contrary, if the side walls are much larger compared to the bottom area (with the top and bottom faces being highly elongated rectangles), the chloroplasts would easily fit into the bottom layer, leaving significant empty space due to inefficient packing and boundary defects, which is suboptimal for the metabolite-production via photosynthesis.

Furthermore, we must consider that the disk-like organelles have an upper bound on their maximal packing density (random close packing), which depends on the confinement, similar to the packing of disks in a plane or spheres in a box (64, 66). Here, we formalize these mathematical upper bounds for I) random close packing and II) the side-to-bottom area mismatch to find the optimal geometry for packing under both constraints. We anticipate that experimental data will fall well below this upper bound, as the disks (chloroplasts) must dynamically rearrange between configurations and, therefore, cannot be strongly jammed.

Constraint (I): Random Close Packing in Confinement. The maximal packing fraction for a disordered arrangement of disks with radii r drawn from a distribution $\mathcal{P}(r)$ in confinement can

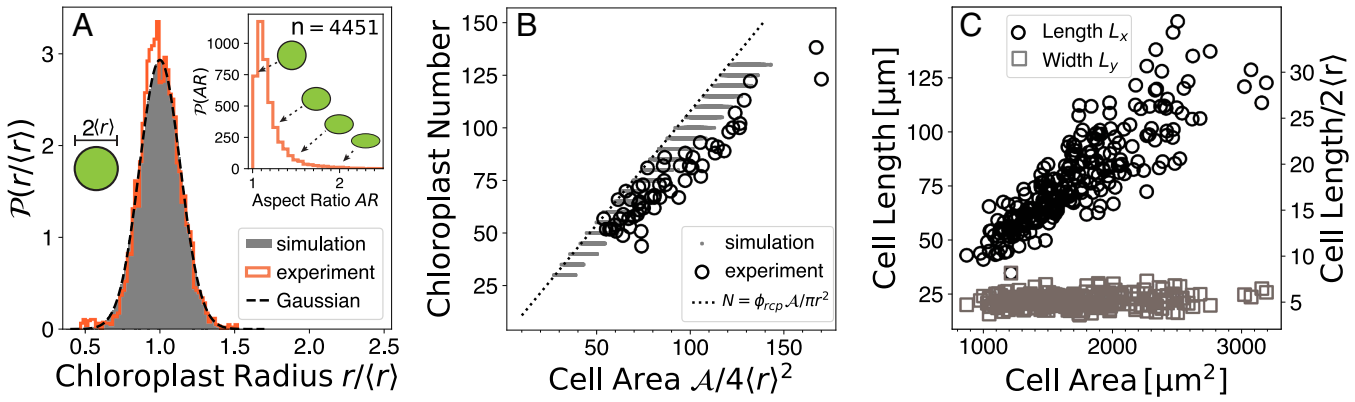

Fig. 2. Chloroplast and cell geometry. (*A*) Gaussian statistics of chloroplast radii in experiments and simulations. Note: Radii are normalized by the mean value, $\langle r\rangle$. *Inset*: The histogram of the aspect ratio shows that experimental chloroplasts are mostly circular. (*B*) Chloroplast number scales with cell area in simulation and experiment. Line depicts expected number for random close packing fraction $\phi_{rcp} = 0.8478$ in free space. (*C*) Larger cells are more elongated (black circles) while having the same width (gray squares). Here, cell-dimensions are normalized with an average chloroplast diameter $2\langle r\rangle = 4.25\,\mu\text{m}$.

be approximated by the random close packing (rcp) fraction ϕ_{rcp}. Although random close packing is not precisely defined and varies depending on the algorithm used (42, 61, 79), we employ this concept to estimate changes in packing density under confinement. Our chloroplast data indicate a Gaussian distribution of radii with a polydispersity of $\delta = \sigma_r/\langle r\rangle = 13.6\%$ (Fig. 2*A*) and a low average aspect ratio, $AR < 1.1$. For a unimodal Gaussian distribution of diameters with such a polydispersity, the random close packing density in asymptotically free space is $\phi_{rcp} \approx 0.841$ (60). The value of the random close packing fraction for confined disks, nonetheless, is less trivial.

We simulate the disk packing in two-sided confinement, L_x and L_y, using an approach adopted from ref. 60 (*Materials and Methods*), which is originally based on the work of Xu et al. (80) and Clarke and Wiley (81), and which has also been applied to one-sided confinement (64). Running 31,904 simulations with varying confinement widths, $L_x = 5.25$ to 37.41 and $L_y = 1.79$ to 11.78, and 1,009 simulations for large aspect ratios for quasi-1D confinement ($L_x = 33.69$ to 126.35) we find that the random close packing fraction, ϕ, depends on both the x- and y-confinement (Fig. 3*A*). We refer to the length scales here as L_x and L_y, expressed in units of the average chloroplast diameter, $2\langle r\rangle$. To explore the variation in random close packing fraction ϕ within a 2D-container under confinement, we use a phenomenological relationship, first introduced in 1946 (82, 83), which has also been applied to 1D confinement (64) and rods in a cylindrical container (84): $\phi = \phi_{rcp} - \alpha(\frac{1}{L_x} + \frac{1}{L_y}) = \phi_{rcp} - \frac{\alpha}{2}\frac{\mathcal{C}}{\mathcal{A}}$. Here, ϕ_{rcp} is the free-space random close packing fraction of the polydisperse disks, $\mathcal{C} = 2(L_x + L_y)$ is the perimeter, and $\mathcal{A} = L_xL_y$ is the box area. However, we observe significant oscillations in packing density under strong confinements, $L_y \lesssim 4$ (Fig. 3 *A* and *B*). These oscillations are similar to commensurability effects also found in confined monodisperse packings and quasi-1D hard-sphere liquids (85, 86) and get enhanced for smaller polydispersity (see *SI Appendix*, Text and Figs. S4 and S5 for details). To precisely model slender cells and especially the packing on the side walls, we extend the simple hyperbolic law by introducing a damped oscillatory correction term (Fig. 3 *A*, *Inset*):

$$\begin{aligned}\phi_I(L_x, L_y) =& \phi_{rcp} - \alpha\left(\frac{1}{L_x} + \frac{1}{L_y}\right) \\ &+ \beta\left(\cos(2\pi(\frac{L_x}{\lambda} - \theta))e^{-L_x/\xi} + \cos(2\pi(\frac{L_y}{\lambda} - \theta))e^{-L_y/\xi}\right)\end{aligned} \quad [1]$$

The oscillatory relation is mainly needed to accurately model the packing on the side walls (x-z and y-z planes in Fig. 1), where one dimension is highly confined ($L_z \approx 2.34$). Fitting this symmetric relation to our simulation data gives $\phi_{rcp} = 0.8482 \pm 2\cdot10^{-4}$ for the free-space random close packing of this disk size distribution, with $\alpha = 0.2659 \pm 5\cdot10^{-4}$, $\beta = 0.109 \pm 0.004$, $\lambda = 0.916 \pm 0.002$, $\theta = 0.282 \pm 0.006$ and $\xi = 1.18 \pm 0.03$.

This constraint serves as a mathematical upper bound for two-dimensional chloroplast packing within the cell. For confinements where $L_i < 1$ ($i \in \{x, y\}$), the relation breaks down as sampling from a Gaussian with an average disk diameter of $2\langle r\rangle = 1$ becomes strongly constrained (bigger disks cannot fit within the box). This reduces the effective average sampled radius, which is instead drawn from a truncated Gaussian distribution: $\langle r\rangle_L = \langle r\rangle - \sigma_r g(x)/\mathcal{G}(x) \approx 0.445$, where $g(x) = \exp(-\frac{x}{2})/\sqrt{2\pi}$, $\mathcal{G}(x) = (1 + \mathrm{erf}(x/\sqrt{2}))/2$, and $x = (L/2 - \langle r\rangle)/\sigma_r$. In our case, this results in a packing fraction for such confinement at $L_y = 1$: $\phi = \pi\langle r\rangle_L^2 \approx 0.622$. This explains the discrepancy of the fitted function Eq. **1** which reaches $\phi_I(1, 1) \approx 0.397$, largely underestimating the sampling-corrected packing fraction. Hence, the estimation of the mean needs to be corrected for very strong confinements, though this correction is not considered here as all length-scales remain $L_i > 1$.

Constraint (II): Area-Side-Wall Mismatch. The ability of chloroplasts to move toward the side walls under strong light introduces a second geometrical constraint on the maximal possible packing fraction.

If the chloroplasts can cover the area $\mathcal{A} = L_xL_y$ at a high packing fraction $\phi_A(L_x, L_y)$, they must also be able to cover the four sidewalls without exceeding the maximal packing fractions ϕ_B and ϕ_C (Fig. 1 *G* and *H*). We obtain the theoretical maximal packing density at the walls, ϕ_B, ϕ_C, approaching the respective random close packing $\phi_B \to \phi_I(L_x - 1, L_z)$ and $\phi_C \to \phi_I(L_y - 1, L_z)$, as described in Eq. **1**. Note that at the side walls, the effective wall length and width are reduced by one chloroplast diameter as the chloroplasts are positioned along the inner walls. If the sidewalls were fully packed and folded into a box, chloroplasts might overlap due to their three-dimensional shape (see Fig. 1 *D*–*F* for comparison). Henceforth, we require that the maximal number of chloroplasts covering the bottom area also fits onto the side walls $N\pi/4 = \phi_A\mathcal{A} \le 2L_z\left(\phi_B\cdot(L_x - 1) + \phi_C\cdot(L_y - 1)\right) = N_{side}\pi/4$. Here, the area of the chloroplast $\pi\langle r\rangle^2$ has been normalized by the area of a square containing it $4\langle r\rangle^2$. Using Eq. **1**, we arrive at

$$\begin{aligned}\phi \le \phi_{II} =& \frac{2L_z}{\mathcal{A}}\left(\phi_I(L_x - 1, L_z)(L_x - 1)\right. \\ &\left. + \phi_I(L_y - 1, L_z)(L_y - 1)\right).\end{aligned} \quad [2]$$

The density ϕ at the bottom is subject to two constraints: I) the geometrically feasible random close packing (Eq. **1**) and II) the available space at the side walls (Eq. **2**). Consequently, the maximal possible packing under both constraints ϕ must satisfy:

$$\phi \le \min(\phi_I, \phi_{II}) \equiv \phi^*. \quad [3]$$

Structural Comparison of Chloroplast Packing and Simulations. We compare simulations and the model ϕ^* to experiments by analyzing the data from 59 cells containing 4,451 chloroplasts to determine whether their structural properties are similar to those of the simulated packing configurations. To this end, we perform a Voronoi-tessellation of the chloroplast positions in confinement (Fig. 3 *C* and *D*). The distribution of Voronoi areas $\mathcal{V}$ shows a slight deviation from the k-Gamma distribution $P(\mathcal{V}) = \frac{k^k}{\Gamma(k)}\frac{(\mathcal{V}-\mathcal{V}_c)^{k-1}}{(\langle\mathcal{V}\rangle-\mathcal{V}_c)^k}\exp\left(-k\frac{\mathcal{V}-\mathcal{V}_c}{\langle\mathcal{V}\rangle-\mathcal{V}_c}\right)$, with a shape parameter k, a cutoff scale $\mathcal{V}_c$ and an average $\langle\mathcal{V}\rangle$.

The comparison with the k-Gamma distribution is primarily done since it represents a maximum entropy law found in various packing structures of granular media and cells (54, 87). While the k-Gamma law closely fits the simulated packing structures (by comparing the cumulative distribution functions (CDF) of data and the theoretical k-Gamma distribution in a P-P plot, see *Inset* of Fig. 3*D*), introducing a small number of random deletions of disks (1% to 20% of the disk number) produces deviations in the probability distribution function similar to that in the experiments (Fig. 3 *C*, *D*, and *H*). This suggests that the measured chloroplast packing is more representative of packing densities below random close packing.

Further, we quantify the p-atic bond-orientational order parameter ($p \in \{4, 5, 6, 7\}$) for each chloroplast j and its N_j

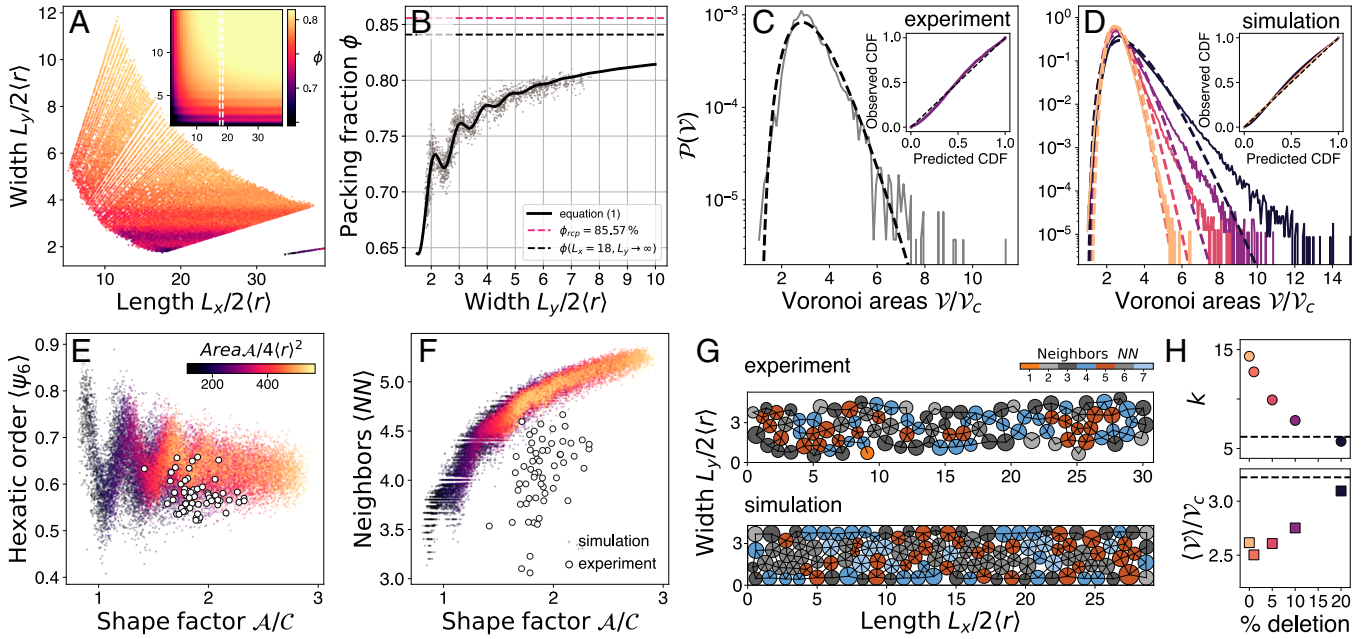

Fig. 3. Packing statistics of simulation and experiment. (*A*) Map of simulated maximal disk packing fraction in respective confinements (L_x, L_y). *Inset*: fit of Eq. **1**. (*B*) Packing fraction of simulation (points) and fit (black solid line) depending on the width L_y, at cell lengths $L_x \in [17, 18.5]$ [dashed white lines in the *Inset* of (*A*)]. Black dashed line: expected asymptotic packing fraction for uniaxial confinement $L_y \to \infty$. Magenta dashed line: expected asymptotic packing fraction in free space. Oscillations are significant at confinements of $L_y/2\langle r\rangle \lesssim 4$. (*C*) Voronoi area distribution of experiment packing follows a k-Gamma distribution (dashed line). *Inset*: P-P plot of cumulative distribution function (CDF) suggests slight variations of observed and maximum entropy (k-Gamma) distribution, suggesting structure. (*D*) Distribution of simulated packings with increasing random deletions of particles (darker colors), indicating that random voids can generate structure. (*E*) Average hexatic order parameter for all confinements, indicated by a shape factor comparing area to perimeter. Color map represents the area. Strong oscillations become apparent in smaller and more elongated cells. White-points: experimental observation. (*F*) The number of nearest neighbors scales with the size and shape of the container. The larger the bulk phase, the more neighbors are allowed. The number of nearest neighbors in experiments significantly underestimates that of the random packings, suggesting more defects and less dense packing. (*G*) Packing in experiments (*Top*) and simulations (*Bottom*), colors indicate the nearest neighbor numbers *NN*. Lines: nearest neighbor network. (*H*) Distribution parameters for shape k and average $\langle\mathcal{V}\rangle$ compared to experiment (dashed line) as a function of the percentage of random deletions. The colors of each point correspond to the data in (*D*).

nearest neighbors, then average the results within each cell

$$\langle\Psi_p\rangle = \langle\frac{1}{N_j}\sum_{k=1}^{N_j} e^{ip\theta_{jk}}\rangle, \qquad [4]$$

where θ_{jk} is the bond-angle between particle j and its nearest neighbor k. Focusing on the hexatic order parameter ($P = 6$) and the number of nearest neighbors (Fig. 3 *E*–*G*), we find that the nearest neighbor number is slightly lower than in the simulations. Additionally, the hexatic order is also slightly below the values from simulations, which has to do with more disordered packing due to the additional space of random deletions and the on average smaller number of nearest neighbors. This suggests a comparable overall structure of the chloroplasts with the model of packing with deletions: a disordered material with a few hexagonal domains (compare also $P = 4, 5, 7$ in *SI Appendix*, Fig. S6). Strikingly, these values are consistent with those reported in ref. 60, where polydispersity was shown to have a strong effect on hexatic order.

Additionally, we find that most packings exhibit an average nearest-neighbor number of $N > 4$ (similar to a coordination number), which is a feature of mechanical stability of jammed structures in two dimensions (42, 88). Next, we use the cell shape data to compare it to the predictions from the model ϕ^*.

Cell Shape Is Optimal for Chloroplast Packing. We represent the coordinates of the field $\phi^*(L_x, L_y, L_z)$ in terms of the dimensionless cell area $\mathcal{A}$ and perimeter $\mathcal{C}$ (Fig. 4*A*), while keeping $L_z = 2.34$ constant. This representation comes with the caveat of an excluded region, as $\mathcal{A} \leq \mathcal{C}^2/16$ for rectangles (the maximal area for a given perimeter corresponds to a square). Intuitively, constraint I) is weaker for larger cells, as a large bulk phase allows for more possibilities of optimized packing (*SI Appendix*, Fig. S7*A*). We can see that $\phi_I \to \phi_{rcp}$ as $L_x, L_y \to \infty$, i.e. for infinitely large boxes.

In contrast, constraint II) is weaker for elongated and small cells, which have a larger sidewall area relative to the bulk area (*SI Appendix* Fig. S7*B*). This is evident by extending only one dimension, $L_x \to \infty$ while $L_y \to 0$, where $\phi_{II} \to \infty$, rendering this constraint irrelevant for very slim and elongated cells. On the contrary, $\phi_{II} \to 0$ when both $L_x, L_y \to \infty$, i.e. a very strong constraint for large boxes.

As both constraints are mutually incompatible, we find a maximum ridge of optimality, where the packing fraction is as large as 81%, which is only 3.7% below rcp in free space (Fig. 4*A*). Intriguingly, the data of cell shapes coincide closely with this maximum ridge, suggesting that cells are compatible with optimal packing density. The measured chloroplast packing fractions (colored points in Fig. 4 and *Inset*) remain well below the expected maximal packing fraction.

In fact, the average packing fraction of approximately 67% ± 6% (mean ± SD) is around 10% below the maximal packing fraction, suggesting that the cells could indeed occupy a larger space in the $\mathcal{C}-\mathcal{A}$-plane without losing much of the geometric benefits, or alternatively, accommodate a higher number of chloroplasts. This discrepancy, however, is expected and can be explained by the difference between the average nearest neighbor distance d

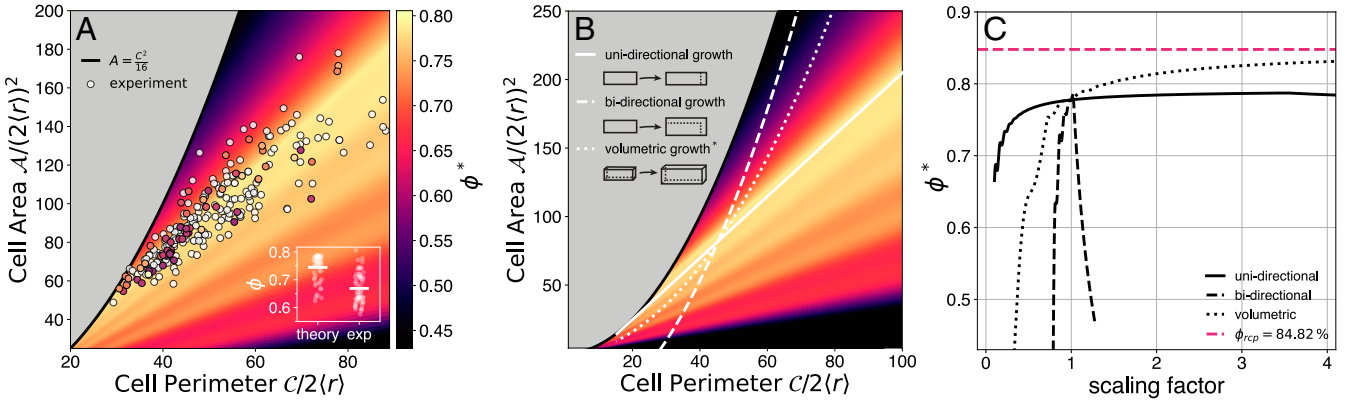

Fig. 4. Maximal packing under geometric constraints. (*A*) Color represents the maximal possible packing fraction ϕ^* according to Eq. **3**. The shaded area is inaccessible to rectangles and exceeds the formula for squares $\mathcal{A} = \mathcal{C}^2/16$. Circles represent individual cells from microscopy experiments, with packing fractions indicated by color. *Inset*: comparison of theoretically expected maximal packing fraction and measured packing fraction for all cells. (*B*) Same field as in (*A*) with extended boundaries. Lines indicate different growth models: uniaxial (solid line, L_x), biaxial (dashed line, L_x,L_y), and volumetric growth models (dotted line, L_x,L_y,L_z). Volumetric up or down-scaling of the cell size is equivalent to down or up-scaling of chloroplast size, respectively. (*C*) Measured maximal packing fraction for the three growth models with corresponding lines. The scaling factor compares the updated to the original cell length: L'_x/L_x. Dashed magenta line: random close packing fraction in free space.

and the chloroplast diameter $\langle d-2r\rangle/2\langle r\rangle = 0.1 \pm 0.05$. Hence, there is a small interchloroplast distance of $l = 0.42 \pm 0.2\,\mu$m, consistent with the previous observations (9). This suggests that chloroplast packing is not organized directly at the random close packing point but slightly below it, allowing for occasional rearrangements of the chloroplasts over larger timescales (9). Additionally, other organelles and structures, invisible to our imaging method, need space, making full chloroplast contact highly unlikely. We note, that both random close packing and glass transition point vary similarly with confinement (70–73), meaning, that while the maximal packing fraction ϕ^* is generally larger than the observed chloroplast arrangements, the structure of the optimality graph remains unaltered for any packing fraction below that value, including the glass transition packing fraction (*SI Appendix*, Fig. S8).

Moreover, we found that some cells exhibit a more irregular height profile, especially when one cell wall of the lower cell layer is aligned with one of the upper cell layers. In such cases, the cell wall can form a deep trench of up to $L_z \approx 4$. Here, the anticlinal wall (facing outward; see Fig. 1*D* and A-side) and the periclinal walls (between the cells Fig. 1*D* and B-side) have approximately the same area and shape. This configuration minimizes the influence of the side wall area as a constraint on the packing fraction.

In the last step, we illustrate lines of growth within the three-variate function $\phi^*(L_x, L_y, L_z)$. We model growth by starting at a specific cell size, close to optimality with $L_x = 18.2$, $L_y = 4.5$ and $L_z = 2.34$, and linearly increasing the size of the axes as $L_i \rightarrow L_i + \alpha_i$, $i \in \{x, y\}$. We model uni- and bidirectional growth by setting α_i to either 0 or a linear growth function in time, $\alpha(t)$, for the i'th direction, respectively. This generates various curves in the $\mathcal{C} - \mathcal{A}$ plane (Fig. 4*B*). Additionally, we scale all axes proportionally in all directions ($L_i \rightarrow \alpha_i L_i$, $\forall i \in \{x, y, z\}$), equivalent to changing the chloroplast size, as studied experimentally (33–39). We monitor how ϕ^* evolves on these curves, noting that volumetric scaling evolves in three dimensions. The corresponding ϕ^* function, dependent on the scaling factor (updated length compared to initial length L'_x/L_x), is shown in Fig. 4*C*. While unidirectional growth allows cells to remain aligned with the maximal ridge of ϕ^*, bidirectional growth quickly deviates from the maximum, resulting in effectively more quadratic cell shapes. Notably, most cells have similar widths but largely different lengths (Fig. 2*C*), suggesting unidirectional cell growth, enabling cells to remain near the maximal ridge during development. Interestingly, volumetric scaling, which is equivalent to changing the size of chloroplasts, can even increase the maximal random close packing fraction ϕ^*. This could explain the observed adaptability enhancement in cells with smaller, more numerous chloroplasts (35, 38), as opposed to intercellular "crowding" (33). Our analysis, therefore, provides a potential framework to understand chloroplast motion and adaptation under confinement and in relation to cell geometry.

Discussion

Packing objects into a confined space is a challenging and ubiquitous problem (40), from candies in a jar to understanding structural configurations in condensed matter systems (42, 89). The problem also extends to practical considerations such as packaging optimization (43) and more abstract scenarios like high-dimensional sphere packing (44, 90), which plays a role in telecommunication and information theory. Notably, biological systems have evolved to tackle packing challenges, from densely packed cells in embryos (51), organoids (91) and tissues (49, 92, 93), bacterial growth in confinement (94), to compactly folded genetic material in nuclei (95, 96).

We show that the packing of mesoscale structures, such as organelles in biological systems, plays a crucial role in adaptation processes. Specifically, we combined structural analysis of photosynthetic chloroplasts in the water plant *E. densa* with disk-packing simulations in confinement to explore the efficiency of chloroplast packing within cells. To cope with the everchanging light conditions, chloroplast rearrangement results in two distinct configurations: high coverage on the bottom cell wall for maximal light absorption in dim conditions and a fast and efficient relocation to the side walls to minimize light exposure under strong light.

First, we investigated the size and shape of cells and chloroplasts. Notably, we found that chloroplasts are Gaussian distributed, which must rely on a size control mechanism. Simple growth-division models with either size-additive noise or size-multiplicative noise predict Gaussian and log-normal

size distributions, respectively (97, 98). However, due to the small coefficient of variation (polydispersity $\delta = 13.6\%$) these two distributions are not distinguishable from each other within the resolution of our data. Additionally, we found that the chloroplast number scales with cell size, consistent with observations in other plants (29, 30, 32). This suggests an intrinsic mechanism that regulates chloroplast number and thus density (99, 100). Furthermore, the cuboid cells display variations in lengths but similar widths and heights, a pattern consistent with unidirectional growth, as expected from development in monocot plants with simple leaf architecture, where growth is predominantly localized near the leaf base (101, 102).

To investigate the optimality of cellular geometry for chloroplast packing, we simulated the random close packing of disks under confinement. The geometry-dependent maximal packing was then compared to a phenomenological packing model, similar to the hyperbolic laws previously applied (64, 82–84), with an added explicit treatment of nonmonotonic deviations under strong confinements ($L \lesssim 4$). This was necessary for accurately evaluating packing on the side walls with heights around $L_z \approx 2.34$. By combining two constraints—maximal packing on the bottom side and all side walls of the box—we constructed a law for cell shape–dependent optimal packing. Mapping measured cell structures to this morphological packing criterion showed that the cuboid cells have optimal shape and dimension to meet these two targets. This morphological feature allows cells to adapt their intracellular structure efficiently for optimized light absorption while simultaneously being able to mitigate potential photodamage by switching between packing configurations. We hypothesize that this trait is likely a result of evolutionary adaptation to the plant's highly fluctuating aquatic environment. Furthermore, this simple physical constraint may also explain the inefficient chloroplast rearrangement observed in various mutant plants with altered chloroplast sizes and numbers (33–39).

While the cell sizes and shapes align well with optimal packing solutions, the experimentally observed densities consistently fall below the shape-dependent maximal packing fraction by up to 10%. Several factors can explain this discrepancy: 1) cells are not perfectly cuboid, and chloroplasts are not perfectly disk-shaped; 2) chloroplasts are embedded within a cellular matrix of other organelles, cytoplasm, and especially cytoskeletal filaments (8, 11), which impose an interchloroplast spacing, suggesting that the effective radius of chloroplasts might be slightly underestimated; and most importantly 3) our previous study (9) suggested that dim-light adapted chloroplasts are close to a two-dimensional supercooled phase, allowing space for rearrangements, especially to facilitate efficient transitions between the two packing configurations. This transition is also accompanied by possible aggregation of chloroplasts into 3D structures that swirl and spread on the side walls. Notably, the 2D packing fractions we found are rather close to a liquid–hexatic transition region (103–105) which also shows reduced hexatic order (Fig. 3*E*) as compared to the dense packing from simulations.

Random close packing lies higher than the glass transition point (106) and produces static packings, however, the critical density for the glass transition in confinement depends similarly on the confinement (73). The measured densities of about 10 to 20% below the random close packing point are in line with previously observed proximity to a glassy phase (9) and due to linearity, replacing ϕ_{rcp} by $\phi_c < \phi_{rcp}$ in Eqs. **1** and **2**, will not alter optimal-shape space (*SI Appendix*, Fig. S8). Additionally, the side-wall mismatch (Eq. **2**) is in many cases not the limiting factor for packing for slightly elongated cells and mostly penalizes square-shaped cells (*SI Appendix*, Fig. S7). As the measured chloroplast density in the bottom layer lies well below the random close packing fraction, the constraint of packing on the sidewalls does also not require a maximal packing. Deviations from the monolayered side-wall packing (such as multilayered packing or aggregates) can also arise from a not perfectly parallel and even light path, due to tissue and cell curvature, and absorption of light in the upper cell layer (*SI Appendix*, Fig. S2).

Overall, our study highlights the importance of packing problems in confinement in biological systems, which might be the key to understanding the collective light-controlled chloroplast rearrangement within plant cells, a physiologically relevant process for light adaptation. Our findings suggest that plant cells develop geometries that balance the motion and rearrangement of organelles inside the cell, while being able to integrate into the tissue. This raises the intriguing question: How are cellular and developmental processes shaped by packing constraints across scales? We note that relatively high packing fractions have been found in land plants such as Spinach and Beetroot (29), Wheat (30) and *Arabidopsis thaliana* (31), which are known to undergo chloroplast motion. Using the presented approach to study the packing and cell-shape optimization in these species would be a natural expansion of this work, which could prove the role of packing density in confinement on the role of chloroplast motion and photoadaptation (32–39).

While it is known that intracellular processes can be modulated via macromolecular crowding (107, 108), we expect that not only organelle size (109) but also the packing configuration of organelles, condensates, and vesicles may play crucial roles for cell physiology, homeostasis and mechanics (110, 111).

To further broaden the scope of our work, we note that we mainly investigated the two chloroplast configurations within the plant cells. However, the transition and coordination of chloroplast motion offer another intriguing direction of research: Chloroplasts can individually sense and move in response to light (8) and yet rearrange collectively by coordinated movements similar to flocks, forming three-dimensional mobile aggregates and spreading along the cell walls. Besides its biological relevance, this rich phenomenology displays fertile ground for future studies, especially from a perspective of phase transitions of confined active matter systems.

Materials and Methods

Imaging and Image Processing. We measured the chloroplast density in three different leaves of *E. densa* plants. For this purpose, we detached healthy leaves from the stem and imaged the bottom layer (abaxial layer) of the tissue. For imaging a Nikon TI2 microscope, a Prime BSI Express sCMOS camera and bright-field illumination using red-color bandpass filter (600 nm, *FWHM* = 40 nm) was used (*SI Appendix*, Fig. S3). Additionally chlorophyll autofluorescence imaging was performed using a CY5 filter cube (excitation: 604 to 644 nm, emission: 672 to 712 nm). To account for the curvature of the leaf tissue, we acquire z-stacks of 10 to 20 μm. Z-stacks were compressed into a single plane by extended depth-of-field-stacking using a Sobel filter approach (kernel width = 10 px) to account for the curvature of the underlying tissue. Chloroplasts were segmented using StarDist (112). Cells are segmented by hand from bright-field images. Segmented chloroplasts are assigned to their cells and filtered by size with an equivalent diameter $d = 2\sqrt{A/\pi}$ in a range of 2 to 15 μm; note that chloroplasts are expected to be around 4 to 6 μm in diameter. Additionally, we require a solidity (area divided by convex hull area) of above 0.7 to ensure mostly convex particles, excluding misdetections. Packing fractions were calculated by

summing chloroplast areas in different cells: $\phi = \sum_{i=1}^{N} A_i/\mathcal{A}$. The p-atic order parameter (Eq. **4**) was calculated from chloroplast positions via a distance matrix D_{ij} and a cutoff depending on chloroplast radii r_i: $d_{ij} = 2(r_i + r_j) + r_a$, where $r_a = 0.4$ represents an additional zone of 20% of the radius around every chloroplast.

We calculate the Voronoi tessellation of chloroplasts within each cell and measure the Voronoi volumes $\mathcal{V}$. We compare the measured histograms with the maximum entropy k-Gamma distribution $P(\mathcal{V}) = \frac{k^k}{\Gamma(k)} \frac{(\mathcal{V}-\mathcal{V}_c)^{k-1}}{(\langle\mathcal{V}\rangle-\mathcal{V}_c)^k} \exp\left(-k\frac{\mathcal{V}-\mathcal{V}_c}{\langle\mathcal{V}\rangle-\mathcal{V}_c}\right)$, where $\mathcal{V}_c \approx \min(\mathcal{V})$ and $k = \frac{\langle\mathcal{V}\rangle-\mathcal{V}_c}{\mathrm{var}(\mathcal{V})}$. Cell shape parameters such as aspect ratio, length scales L_x and L_y, area $\mathcal{A}$ and perimeter $\mathcal{C}$ are calculated from the mask images.

Confocal Imaging and Image Processing. We mount an *Elodea* leaf on a microscope slide with a spacer, remove the water from the aquarium culture, and immerse it in a mixture of one drop (approx 100 μl) Calcofluor White Stain (MERCK) and one drop of 10% potassium hydroxide, subsequently we place a coverslide. Calcofluor is used to stain cellulose in the cell walls (113). Confocal imaging is performed with a Leica SP8 in the Leeuwenhoek Centre for Advanced Microscopy, Amsterdam. A 405 nm diode laser is used for the excitation of Calcofluor White, and the emission band is set from 450 to 520 nm. Chlorophyll autofluorescence is excited with a Helium Neon laser at the 633 nm line, and the emission band ranges from 640 to 740 nm. We acquire z-stacks of 0.36 μm step size with a x-y pixel size of 0.3 μm using a 60× oil-immersion objective (NA = 1.4). For processing, the Calcofluor channel is first slightly blurred using a Gaussian filter ($\sigma = 1$ px), then binarized using Li's method in FIJI (114), then inverted (i.e. cells interior is 1 and cell walls 0). Subsequent morphological opening using a cube of 2 pixels and distance-transform watershed segmentation using Manhattan-metric and a 6-connectivity generated to a well-separated label map for cells. Subsequently, we rejected labels touching the upper or lower boundary of the field of view, enabling us to avoid segmentation of the upper cell layer and noisy background. We measure the average height in the border of all cells within one chloroplast diameter $2\langle r\rangle \approx 4.25$ μm from the side wall.

Disk Packing Algorithm. We use a disk packing algorithm based on previous works (80, 81) and further modified and applied in refs. 60 and 64. In brief, we first select a fixed number of particles N drawn from a size distribution $P(r)$, with $P(r)$ chosen to be a Gaussian with polydispersity $\delta = 13.6\%$ to match the experiments. The N particles are randomly placed in a confined system with initial size L_x and L_y such that the initial area fraction $\phi = 0.01$ and no particles are allowed to overlap. We then loop through the particles in random order, trying to expand each particle's size by a small amount a, if that expansion does not cause any overlap with other particles or with the walls of the system. We additionally try to move each particle a small distance in a random direction, again only if that displacement does not cause an overlap. When all particles have been successfully expanded by a, the system size is rescaled ($L_x' = L_x/a$, $L_y' = L_y/a$), particle sizes rescaled down by a, and particle positions within the box likewise rescaled. If too many trials occur without every particle successfully expanding, then the particle sizes are reset to the last rescaled value, a is decreased, and the trials resume. This continues until $a - 1 = 10^{-5}$, at which point the simulation is concluded. Throughout the simulation, the aspect ratio L_x/L_y is kept fixed, so to explore the necessary conditions, we vary N from 30 to 130 and L_x/L_y from 1.0 to 10.0. Additionally, simulations of boxes with periodic boundary conditions at aspect ratio 20 are performed to resolve the unilaterally confined limit. For polydispersity $\delta = 13.6\%$, we run 32,913 simulations, with at least 5 repetitions of each condition and in many cases more. To evaluate the effect of polydispersity we run additional simulations ($n = 56{,}312$) in the above mentioned L_x and L_y domains for polydispersity $\delta = 2.5\%$, 5%, 7.5%, 10%, 12%, and 16% (*SI Appendix*, Text and Figs. S4 and S5).

Data, Materials, and Software Availability. Microscopy and simulation data have been deposited in Zenodo (115).

ACKNOWLEDGMENTS. We extend our gratitude to Karen Villari for her contributions to obtaining cell shape images. We also thank Ronald Breedijk for his assistance with confocal microscopy at the Leeuwenhoek Centre for Advanced Microscopy, Amsterdam. Additionally, we thank Max Bi, Kartik Chhajed, Marko Popović, Isabelle Eisenmann, Yuri Z. Sinzato, and Jared Popowski for insightful discussions. M.J. acknowledges support from the European Research Council Grant No. "2023-StG-101117025, FluMAB." This publication is part of the Vidi project *Living Levers* with file No. 21239, financed by the Dutch Research Council (NWO).This material is based on work supported by the NSF under Grant No. CBET-2306371 (E.R.W.).

1. Y. Forterre, Slow, fast and furious: Understanding the physics of plant movements. *J. Exp. Bot.* **64**, 4745–4760 (2013).
2. Y. Meroz, R. Bastien, L. Mahadevan, Spatio-temporal integration in plant tropisms. *J. R. Soc. Interface* **16**, 20190038 (2019).
3. D. E. Moulton, H. Oliveri, A. Goriely, Multiscale integration of environmental stimuli in plant tropism produces complex behaviors. *Proc. Natl. Acad. Sci. U.S.A.* **117**, 32226–32237 (2020).
4. C. Nguyen *et al*., Noisy circumnutations facilitate self-organized shade avoidance in sunflowers. *Phys. Rev. X* **14**, 31027 (2024).
5. A. Geitmann, A. Nebenführ, Navigating the plant cell: Intracellular transport logistics in the green kingdom. *Mol. Biol. Cell* **26**, 3373–3378 (2015).
6. M. Kasahara *et al*., Chloroplast avoidance movement reduces photodamage in plants. *Nature* **420**, 829–832 (2002).
7. P. A. Davis, S. Caylor, C. W. Whippo, R. P. Hangarter, Changes in leaf optical properties associated with light-dependent chloroplast movements. *Plant, Cell Environ.* **34**, 2047–2059 (2011).
8. M. Wada, S. G. Kong, Actin-mediated movement of chloroplasts. *J. Cell Sci.* **131**, jcs210310 (2018).
9. N. Schramma, C. Perugachi Israëls, M. Jalaal, Chloroplasts in plant cells show active glassy behavior under low-light conditions. *Proc. Natl. Acad. Sci. U.S.A.* **120**, e2216497120 (2023).
10. N. Schramma, G. C. Canales, M. Jalaal, Light-regulated chloroplast morphodynamics in a single-celled dinoflagellate. *Proc. Natl. Acad. Sci. U.S.A.* **121**, 1–9 (2024).
11. A. Kadota *et al*., Short actin-based mechanism for light-directed chloroplast movement in *Arabidopsis*. *Proc. Natl. Acad. Sci. U.S.A.* **106**, 13106–13111 (2009).
12. N. Suetsugu *et al*., Two kinesin-like proteins mediate actin-based chloroplast movement in *Arabidopsis thaliana*. *Proc. Natl. Acad. Sci. U.S.A.* **107**, 8860–8865 (2010).
13. M. E. Dwyer, R. P. Hangarter, Light-induced displacement of PLASTID MOVEMENT IMPAIRED1 precedes light-dependent chloroplast movements. *Plant Physiol.* **189**, 1866–1880 (2022).
14. M. Wada *et al*., Chloroplast-actin filaments decide the direction of chloroplast avoidance movement under strong light in *Arabidopsis thaliana*. *J. Plant Res.* **137**, 659–667 (2024).
15. S. G. Kong *et al*., Chloroplast unusual positioning 1 is a plant-specific actin polymerization factor regulating chloroplast movement. *Plant Cell* **36**, 1159–1181 (2024).
16. G. Senn, *Die Gestalts-und Lageveränderung der Pflanzen-Chromatophoren: Mit Einer Beilage: Die Lichtbrechung der Lebenden Pflanzenzelle* (W. Engelmann, 1908).
17. J. Zurzycki, The influence of chloroplast displacements on the optical properties of leaves. *Acta Soc. Bot. Pol.* **30**, 503–527 (1961).
18. E. Gotoh *et al*., Chloroplast accumulation response enhances leaf photosynthesis and plant biomass production. *Plant Physiol.* **178**, 1358–1369 (2018).
19. Y. I. Park, W. S. Chow, J. M. Andersen, Chloroplast movement in the shade plant *Tradescantia albiflora* helps protect photosystem II against light stress. *Plant Physiol.* **111**, 867–875 (1996).
20. A. V. Ruban, Plant in light. *Commun. Integr. Biol.* **2**, 50–55 (2009).
21. Z. Li, S. Wakao, B. B. Fischer, K. K. Niyogi, Sensing and responding to excess light. *Annu. Rev. Plant Biol.* **60**, 239–260 (2009).
22. O. Sztatelman, A. Waloszek, A. Katarzyna Banaś, H. Gabryś, Photoprotective function of chloroplast avoidance movement: In vivo chlorophyll fluorescence study. *J. Plant Physiol.* **167**, 709–716 (2010).
23. P. A. Davis, R. P. Hangarter, Chloroplast movement provides photoprotection to plants by redistributing PSII damage within leaves. *Photosynth. Res.* **112**, 153–161 (2012).
24. C. W. Whippo *et al*., THRUMIN1 is a light-regulated actin-bundling protein involved in chloroplast motility. *Curr. Biol.* **21**, 59–64 (2011).
25. J. H. Ryu, S. Takagi, R. Nagai, Stationary organization of the actin cytoskeleton in *Vallisneria*: The role of stable microfilaments at the end walls. *J. Cell Sci.* **108**, 1531–1539 (1995).
26. Y. Sakai, S. Takagi, Reorganized actin filaments anchor chloroplasts along the anticlinal walls of *Vallisneria* epidermal cells under high-intensity blue light. *Planta* **221**, 823–830 (2005).
27. Y. Sakai, S. I. Inoue, A. Harada, K. I. Shimazaki, S. Takagi, Blue-light-induced rapid chloroplast de-anchoring in *Vallisneria* epidermal cells. *J. Integr. Plant Biol.* **57**, 93–105 (2015).
28. Y. Sakai, S. Takagi, Roles of actin cytoskeleton for regulation of chloroplast anchoring. *Plant Signal. Behav.* **12**, e1370163 (2017).
29. S. I. Honda, T. Hongladarom-Honda, P. Kwanyuen, S. G. Wildman, Interpretations on chloroplast reproduction derived from correlations between cells and chloroplasts. *Planta* **97**, 1–15 (1971).
30. J. Ellis, R. Leech, Cell size and chloroplast size in relation to chloroplast replication in light-grown wheat leaves. *Planta* **165**, 120–125 (1985).
31. K. W. Osteryoung, K. D. Stokes, S. M. Rutherford, A. L. Percival, W. Y. Lee, Chloroplast division in higher plants requires members of two functionally divergent gene families with homology to bacterial ftsZ. *Plant Cell* **10**, 1991–2004 (1998).
32. K. A. Pyke, R. M. Leech, Chloroplast division and expansion is radically altered by nuclear mutations in *Arabidopsis thaliana*. *Plant Physiol.* **99**, 1005–1008 (1992).
33. D. C. McCain, Chloroplast movement can be impeded by crowding. *Plant Sci.* **135**, 219–225 (1998).

34. M. Königer, J. A. Delamaide, E. D. Marlow, G. C. Harris, *Arabidopsis thaliana* leaves with altered chloroplast numbers and chloroplast movement exhibit impaired adjustments to both low and high light. *J. Exp. Bot.* **59**, 2285–2297 (2008).
35. W. J. Jeong *et al*., A large population of small chloroplasts in tobacco leaf cells allows more effective chloroplast movement than a few enlarged chloroplasts. *Plant Physiol.* **129**, 112–121 (2002).
36. S. Dutta *et al*., Non-invasive, whole-plant imaging of chloroplast movement and chlorophyll fluorescence reveals photosynthetic phenotypes independent of chloroplast photorelocation defects in chloroplast division mutants. *Plant J.* **84**, 428–442 (2015).
37. S. Dutta *et al*., Variations in chloroplast movement and chlorophyll fluorescence among chloroplast division mutants under light stress. *J. Exp. Bot.* **68**, 3541–3555 (2017).
38. D. Xiong, J. Huang, S. Peng, Y. Li, A few enlarged chloroplasts are less efficient in photosynthesis than a large population of small chloroplasts in *Arabidopsis thaliana*. *Sci. Rep.* **7**, 1–12 (2017).
39. K. Głowacka *et al*., Is chloroplast size optimal for photosynthetic efficiency?. *New Phytol.* **239**, 2197–2211 (2023).
40. T. Aste, D. Weaire, *The Pursuit of Perfect Packing* (Taylor & Francis, 2008), vol. 1, p. 2.
41. S. Torquato, Y. Jiao, Robust algorithm to generate a diverse class of dense disordered and ordered sphere packings via linear programming. *Phys. Rev. E: Stat. Nonlinear, Soft Matter Phys.* **82**, 1–14 (2010).
42. S. Torquato, F. H. Stillinger, Jammed hard-particle packings: From Kepler to Bernal and beyond. *Rev. Mod. Phys.* **82**, 2633–2672 (2010).
43. K. A. Dowsland, W. B. Dowsland, Packing problems. *Eur. J. Oper. Res.* **56**, 2–14 (1992).
44. C. E. Shannon, A mathematical theory of communication. *Bell Syst. Tech. J.* **27**, 379–423 (1948).
45. N. J. Sloane, The packing of spheres. *Sci. Am.* **250**, 116–125 (1984).
46. J. Kepler, *Strena Seu de Nive Sexangula* (Godfried Tampach, Frankfurt am Main, Germany, 1611).
47. T. C. Hales, Historical overview of the Kepler conjecture. *Discret. Comput. Geom.* **36**, 5–20 (2006).
48. T. C. Hales, A proof of the kepler conjecture. *Ann. Math.* **136**, 1065–1185 (2005).
49. A. K. Classen, K. I. Anderson, E. Marois, S. Eaton, Hexagonal packing of *Drosophila* wing epithelial cells by the planar cell polarity pathway. *Dev. Cell* **9**, 805–817 (2005).
50. P. Y. Gires, M. Thampi, S. W. Krauss, M. Weiss, Exploring generic principles of compartmentalization in a developmental in vitro model. *Development (Cambridge)* **150**, dev200851 (2023).
51. D. Fabrèges *et al*., Temporal variability and cell mechanics control robustness in mammalian embryogenesis. *Science* **386**, 1–21 (2024).
52. R. J. Ross *et al*., Hyperdisordered cell packing on a growing surface. *Phys. Rev. X* **15**, 21064 (2025).
53. D. J. Skinner, H. Jeckel, A. C. Martin, K. Drescher, J. Dunkel, Topological packing statistics of living and nonliving matter. *Sci. Adv.* **9**, eadg1261 (2023).
54. T. C. Day *et al*., Cellular organization in lab-evolved and extant multicellular species 2 obeys a maximum entropy law. *eLife* **11**, 1–28 (2021).
55. A. Srinivasan, S. S. M. H. Höhn, R. E. Goldstein, Point processes and the statistics of cellular neighborhoods in simple multicellular organisms. arXiv [Preprint] (2023). https://doi.org/10.48550/arXiv.2311.11939 (Accessed 20 December 2023).
56. L. K. Roth, H. M. Jaeger, Optimizing packing fraction in granular media composed of overlapping spheres. *Soft Matter* **12**, 1107–1115 (2016).
57. Y. Yuan, L. Liu, Y. Zhuang, W. Jin, S. Li, Coupling effects of particle size and shape on improving the density of disordered polydisperse packings. *Phys. Rev. E: Stat. Nonlinear, Soft Matter Phys.* **98**, 42903 (2018).
58. D. S. Shimamoto, M. Yanagisawa, Common packing patterns for jammed particles of different power size distributions. *Phys. Rev. Res.* **5**, 1–6 (2023).
59. C. Anzivino *et al*., Estimating random close packing in polydisperse and bidisperse hard spheres via an equilibrium model of crowding. *J. Chem. Phys.* **158**, 044901 (2023).
60. D. J. Meer, I. Galoustian, J. G. D. F. Manuel, E. R. Weeks, Estimating random close packing density from circle radius distributions. *Phys. Rev. E: Stat. Nonlinear, Soft Matter Phys.* **109**, 1–11 (2024).
61. S. Torquato, T. M. Truskett, P. G. Debenedetti, Is random close packing of spheres well defined? *Phys. Rev. Lett.* **84**, 2064–2067 (2000).
62. P. Chaudhuri, L. Berthier, S. Sastry, Jamming transitions in amorphous packings of frictionless spheres occur over a continuous range of volume fractions. *Phys. Rev. Lett.* **104**, 1–4 (2010).
63. M. Hermes, M. Dijkstra, Jamming of polydisperse hard spheres: The effect of kinetic arrest. *Europhys. Lett.* **89**, 38005 (2010).
64. K. W. Desmond, E. R. Weeks, Random close packing of disks and spheres in confined geometries. *Phys. Rev. E: Stat. Nonlinear, Soft Matter Phys.* **80**, 1–11 (2009).
65. K. V. Edmond, C. R. Nugent, E. R. Weeks, Influence of confinement on dynamical heterogeneities in dense colloidal samples. *Phys. Rev. E: Stat. Nonlinear, Soft Matter Phys.* **85**, 1–10 (2012).
66. D. Chen, S. Torquato, Confined disordered strictly jammed binary sphere packings. *Phys. Rev. E: Stat. Nonlinear, Soft Matter Phys.* **92**, 1–11 (2015).
67. C. O. Solano-cabrera *et al*., Self-assembly and transport phenomena of colloids: Confinement and geometrical effects. *Annu. Rev. Condens. Matter Phys.* **16**, 41–59 (2025).
68. J. Klein, E. Kumacheva, Confinement-induced phase transitions in simple liquids. *Science* **269**, 816–819 (1995).
69. W. K. Kegel, Freezing of hard spheres in confinement. *J. Chem. Phys.* **115**, 6538–6549 (2001).
70. C. R. Nugent, K. V. Edmond, H. N. Patel, E. R. Weeks, Colloidal glass transition observed in confinement. *Phys. Rev. Lett.* **99**, 1–4 (2007).
71. S. Lang *et al*., Glass transition in confined geometry. *Phys. Rev. Lett.* **105**, 1–4 (2010).
72. S. Lang, R. Schilling, V. Krakoviack, T. Franosch, Mode-coupling theory of the glass transition for confined fluids. *Phys. Rev. E: Stat. Nonlinear, Soft Matter Phys.* **86**, 1–14 (2012).
73. S. Mandal *et al*., Multiple reentrant glass transitions in confined hard-sphere glasses. *Nat. Commun.* **5**, 1–8 (2014).
74. G. Jung, T. Franosch, Computer simulations and mode-coupling theory of glass-forming confined hard-sphere fluids. *Phys. Rev. E* **107**, 1–14 (2023).
75. N. Rascio, P. Mariani, E. Tommasini, M. Bodner, W. Larcher, Photosynthetic strategies in leaves and stems of *Egeria densa*. *Planta* **185**, 297–303 (1991).
76. T. Hara *et al*., Organ-level analysis of idioblast patterning in *Egeria densa* planch Leaves. *PLoS ONE* **10**, 1–18 (2015).
77. R. Ligrone, K. C. Vaughn, N. Rascio, A cytochemical and immunocytochemical analysis of the wall labyrinth apparatus in leaf transfer cells in *Elodea canadensis*. *Ann. Bot.* **107**, 717–722 (2011).
78. R. Nagai, Regulation of intracellular movements in plant cells by environmental stimuli. *Int. Rev. Cytol.* **145**, 251–310 (1993).
79. S. Atkinson, F. H. Stillinger, S. Torquato, Existence of isostatic, maximally random jammed monodisperse hard-disk packings. *Proc. Natl. Acad. Sci. U.S.A.* **111**, 18436–18441 (2014).
80. N. Xu, J. Blawzdziewicz, C. S. O'Hern, Random close packing revisited: Ways to pack frictionless disks. *Phys. Rev. E: Stat. Nonlinear, Soft Matter Phys.* **71**, 1–9 (2005).
81. A. S. Clarke, J. D. Wiley, Numerical simulation of the dense random packing of a binary mixture of hard spheres: Amorphous metals. *Phys. Rev. B* **35**, 7350–7356 (1987).
82. L. Verman, S. Banerjee, Effect of container walls on packing density of particles. *Nature* **157**, 584 (1946).
83. R. Brown, P. Hawksley, Effect of container walls on packing density of particles. *Nature* **157**, 585 (1946).
84. J. O. Freeman *et al*., Random packing of rods in small containers. *Granul. Matter* **21**, 1–11 (2019).
85. M. Z. Yamchi, S. S. Ashwin, R. K. Bowles, Inherent structures, fragility, and jamming: Insights from quasi-one-dimensional hard disks. *Phys. Rev. E: Stat. Nonlinear, Soft Matter Phys.* **91**, 1–12 (2015).
86. M. J. Godfrey, M. A. Moore, Understanding the ideal glass transition: Lessons from an equilibrium study of hard disks in a channel. *Phys. Rev. E: Stat. Nonlinear, Soft Matter Phys.* **91**, 1–15 (2015).
87. T. Aste, T. Di Matteo, Emergence of Gamma distributions in granular materials and packing models. *Phys. Rev. E: Stat. Nonlinear, Soft Matter Phys.* **77**, 1–8 (2008).
88. J. Mason, J. D. Bernal, Packing of spheres: Co-ordination of randomly packed spheres. *Nature* **188**, 910–911 (1960).
89. C. P. Royall *et al*., Colloidal hard spheres: Triumphs, challenges and mysteries. *Rev. Mod. Phys.* **96**, 45003 (2023).
90. M. S. Viazovska, The sphere packing problem in dimension 8. *Ann. Math.* **185**, 991–1015 (2017).
91. T. H. Tan *et al*., Emergent chirality in active solid rotation of pancreas spheres. *PRX Life* **2**, 1–28 (2024).
92. R. Farhadifar, J. C. Röper, B. Aigouy, S. Eaton, F. Jülicher, The influence of cell mechanics, cell–cell interactions, and proliferation on epithelial packing. *Curr. Biol.* **17**, 2095–2104 (2007).
93. Y. Tang, X. Li, D. Bi, Tunable hyperuniformity in cellular structures. arXiv [Preprint] (2024). https://arxiv.org/abs/2408.08976 (Accessed 20 August 2024).
94. M. Sreepadmanabh *et al*., Cell shape affects bacterial colony growth under physical confinement. *Nat. Commun.* **15**, 9561 (2024).
95. M. Webster, K. L. Witkin, O. Cohen-Fix, Sizing up the nucleus: Nuclear shape, size and nuclear-envelope assembly. *J. Cell Sci.* **122**, 1477–1486 (2009).
96. E. S. Doğan, C. Liu, Three-dimensional chromatin packing and positioning of plant genomes. *Nat. Plants* **4**, 521–529 (2018).
97. A. Amir, Cell size regulation in bacteria. *Phys. Rev. Lett.* **112**, 208102 (2014).
98. P. Y. Ho, J. Lin, A. Amir, Modeling cell size regulation: From single-cell-level statistics to molecular mechanisms and population-level effects. *Annu. Rev. Biophys.* **47**, 251–271 (2018).
99. K. A. Pyke, Plastid division and development. *Plant Cell* **11**, 549–556 (1999).
100. L. Cackett, L. H. Luginbuehl, T. B. Schreier, E. Lopez-Juez, J. M. Hibberd, Chloroplast development in green plant tissues: The interplay between light, hormone, and transcriptional regulation. *New Phytol.* **233**, 2000–2016 (2022).
101. J. Mathur, Cell shape development in plants. *Trends Plant Sci.* **9**, 583–590 (2004).
102. H. Nelissen, N. Gonzalez, D. Inzé, Leaf growth in dicots and monocots: So different yet so alike. *Curr. Opin. Plant Biol.* **33**, 72–76 (2016).
103. A. H. Marcus, S. A. Rice, Observations of first-order liquid-to-hexatic and hexatic-to-solid phase transitions in a confined colloid suspension. *Phys. Rev. Lett.* **77**, 2577–2580 (1996).
104. E. P. Bernard, W. Krauth, Two-step melting in two dimensions: First-order liquid-hexatic transition. *Phys. Rev. Lett.* **107**, 1–4 (2011).
105. H. Liu, Global equation of state and the phase transitions of the hard disc system. *Mol. Phys.* **119**, e1905897 (2021).
106. R. Ni, M. A. Stuart, M. Dijkstra, Pushing the glass transition towards random close packing using self-propelled hard spheres. *Nat. Commun.* **4**, 1–7 (2013).
107. J. Van Den Berg, A. J. Boersma, B. Poolman, Microorganisms maintain crowding homeostasis. *Nat. Rev. Microbiol.* **15**, 309–318 (2017).
108. L. J. Holt, M. Delarue, Macromolecular crowding: Sensing without a sensor. *Curr. Opin. Cell Biol.* **85**, 102269 (2023).
109. W. F. Marshall, Scaling of subcellular structures. *Annu. Rev. Cell Dev. Biol.* **36**, 219–236 (2020).
110. R. Chang, M. Prakash, Topological damping in an ultrafast giant cell. *Proc. Natl. Acad. Sci. U.S.A.* **120**, 1–12 (2023).
111. J. Chen, M. Mirvis, A. Ekman, B. Vanslembrouck, M. L. Gros, Automated segmentation of soft X-ray tomography: Native cellular structure with sub-micron resolution at high throughput for whole-cell quantitative imaging in yeast. bioRxiv [Preprint] (2024). https://doi.org/10.1101/2024.10.31.621371 (Accessed 12 February 2025).
112. M. Weigert, U. Schmidt, R. Haase, K. Sugawara, G. Myers, "Star-convex polyhedra for 3D object detection and segmentation in microscopy" in *Proceedings of the 2020 IEEE Winter Conference on Applications of Computer Vision, WACV 2020* (2020), pp. 3655–3662.
113. A. J. Bidhendi, Y. Chebli, A. Geitmann, Fluorescence visualization of cellulose and pectin in the primary plant cell wall. *J. Microsc.* **278**, 164–181 (2020).
114. J. Schindelin *et al*., Fiji: An open-source platform for biological-image analysis. *Nat. Methods* **9**, 676–682 (2012).
115. N. Schramma, Dataset: Optimal disk packing of chloroplasts in plant cells. Zenodo. https://doi.org/10.5281/zenodo.17183225. Deposited 4 October 2025.